Analytical Methods

ROYAL SOCIETY OF CHEMISTRY

PAPER

View Article Online
View Journal | View Issue

Cite this: *Anal. Methods*, 2020, **12**, 3883

Simultaneous determination of ascorbic acid, uric acid and dopamine using silver nanoparticles and copper monoamino-phthalocyanine functionalised acrylate polymer†

Zina Fredj,[ab] Mounir Ben Ali,[ab] Mohammed Nooredeen Abbas[c] and Eithne Dempsey *[d]

A silver nanoparticle and copper monoamino-phthalocyanine-acrylate (Cu-MAPA) polymer modified glassy carbon electrode was developed for the simultaneous detection of dopamine (DOP), ascorbic acid (AA) and uric acid (UA) using voltammetric techniques. Silver nanoparticles (AgNPs) were synthesised according to the citrate reduction method. Following synthesis and characterisation the copper phthalocyanine polymer was co-deposited with AgNPs realising a surface with enhanced electron transfer which lowered the overpotential required for analyte electro-oxidation. Differential pulse voltammetry (DPV) was employed for the simultaneous determination of dopamine (DOP), ascorbic acid (AA) and uric acid (UA) at AgNP/Cu-MAPA modified surfaces at <μM ranges. The peak potential separations for DOP-AA and DOP-UA were *ca.* 181 mV and 168 mV respectively. The chemical sensor was also capable of individual quantitation of DOP, UA and AA with detection limits of 0.7, 2.5 and 5.0 nM respectively. Overall, the approach realised a simple and effective electrode modifier for the selective discrimination and quantitation of DOP in the presence of physiological levels of AA and UA.

Received 17th June 2020
Accepted 21st July 2020

DOI: 10.1039/d0ay01183e

rsc.li/methods

1. Introduction

Neurotransmitters dopamine (DOP), ascorbic acid (AA) and uric acid (UA) coexist in biological samples and changes in their concentration levels beyond the critical limits may lead to several health disorders.[1] Ascorbic acid (AA) has various physiological and pharmacological functions, in collagen synthesis, intestinal absorption of iron, and drug metabolism.[2] Moreover, ascorbic acid has been investigated for the prevention and treatment of the common cold and in relation to mental illness, infertility and cancer.[3] Uric acid (UA) is a nitrogenous compound found in urine and it is a product of purine metabolism in the human body. High levels lead to many clinical disorders[4] (*e.g.* hyperuricemia or Lesch–Nyhan syndrome) and are linked with gout, kidney and cardiac problems.[5] For these reasons, analytical devices, which enable signal discrimination and simultaneous detection of these species is of critical importance not only in the field of biomedical chemistry and neurochemistry but also for diagnostic and pathological research. A major obstacle in monitoring DA and UA using electrochemical techniques is the coexistence of AA, which demonstrates strong overlapping electrooxidation signals.[6] Metallic nanoparticle-based voltammetric detection has drawn intense attention in this regard,[7] and among the noble metals, silver nanoparticles (AgNPs) are widely utilised in material science, physics, and chemistry due to particular optical, magnetic, electronic, and catalytic properties.[8]

Zhang and Jiang prepared a gold nanoparticle modified electrode for the electrocatalytic oxidation of AA in the presence of DOP where voltammetric waves of AA and DOP were resolved into two well-defined peaks.[9] H. Vidya *et al.* used silver nanoparticle modified carbon paste electrode (MCPE) for the detection of dopamine[10] and the developed approach was simple and effective for the determination of DA in the presence of AA and UA in the mM range. In addition, Khalilzadeh *et al.* reported the green synthesis of AgNPs for electrochemical detection of ascorbic acid using impedance spectroscopy (EIS).[11] The selectivity and antifouling ability of silver nanoparticle-decorated reduced graphene oxide modified electrodes proved to be an effective means of simultaneous determination of AA, DOP and UA as reported by Balwinder Kaur *et al.*[12] Pd–Ag bimetallic nanoparticles deposited on reduced graphene oxide support were reported for acetaminophen quantitation[13] while the same

[a]*University of Sousse, Higher Institute of Applied Sciences and Technology of Sousse, GREENS-ISSAT, 4003 Ibn Khaldoun Sousse, Tunisia*

[b]*NANOMISENE Lab, LR16CRMN01, Centre for Research on Microelectronics and Nanotechnology of Sousse, Technopole of Sousse, Sahloul, Sousse, 4034, Tunisia*

[c]*Electroanalytical Laboratory, National Research Centre, Cairo, Egypt*

[d]*Department of Chemistry, Maynooth University, Maynooth, Co. Kildare, Ireland. E-mail: eithne.dempsey@mu.ie*

† Electronic supplementary information (ESI) available. See DOI: 10.1039/d0ay01183e

team prepared bimetallic Pt–Ni nanocatalysts with a uniform dispersion on a rGO support using an ethylene glycol reduction method. Compared with the GCE, both Ni/rGO/GCE and Pt/rGO/GCE as well as Pt–Ni/rGO/GCE conducting materials exhibit superior electrocatalytic activity towards the dopamine redox reaction.[14]

Phthalocyanines (Pc) can adopt >70 different metallic and non-metallic ions into the ring cavity,[15] providing great variety and functionality either by substituting different metal atoms into the ring or by altering peripheral and axial functionalities. This substitution facilitates the tailoring of physical parameters of metallophthalocyanines (MPcs) over a broad range and consequently, allows modulation of the physical, electrical and optical behaviour of the compounds. Metallophthalocyanines represent a large family of materials with a centrosymmetric planar structure of 16 member rings with 18 delocalised π-electrons which leads to optical properties and extraordinary stability.[16,17] Recent reports have demonstrated that a cobalt(II) phthalocyanine modified glassy carbon electrode has excellent electrocatalytic activity towards the simultaneous detection of dopamine and ascorbic acid.[18,19] In this context, our team have reported a novel sensor based on immobilised copper phthalocyanine, 2,9,16,23-tetracarboxylic acid-polyacrylamide for determination of acid phosphatase (ACP) levels in nanomolar quantities.[20]

Moreover, S. Pakapongpan *et al.* have used copper(II) phthalocyanine to develop a novel sensor successfully applied to determination of AA in real samples with good performance.[21] R. Seoudi and H. A. Althagafi reported that a mixture of copper phthalocyanine (CuPc) with silver nanoparticles improved the efficiency of a modified layer with an enhancement of optical and electronic properties due to the presence of AgNPs, (relative to the that of AgNPs or CuPc alone).[22] The use of copper phthalocyanine is based on very attractive properties which allow it to be used in many fields as the dyes and pigments, nonlinear optics and in photodynamic therapy of cancer. One of the interesting features of phthalocyanine is their ability to generate cytotoxic singlet oxygen responsible for the destruction of many recalcitrant pollutants in waste water, and in the destruction of cancer cells.[23] On the other hand, nanoparticles have been reported to enhance the photocatalytic activity and singlet oxygen quantum yields of the phthalocyanine.[24] Recently, AuNPs and phthalocyanines have been successfully combined to obtain electrochemical sensors with improved electrocatalytic properties.[25,26] In this work, phthalocyanines are employed in the presence of silver nanoparticles to develop a novel approach for the simultaneous detection of dopamine, uric acid and ascorbic acid. The incorporation of AgNPs may improve the catalytic properties of the electrochemical and electrical impedance system as demonstrated by Alessio *et al.*[27]

In this work, the selective quantitation of dopamine, uric acid and ascorbic acid was achieved *via* co-deposition of AgNPs and a new copper monoamino-phthalocyanine functionalised acrylate polymer as modifiers on glassy carbon transducers. The aim is advancement of analytical sensing performance in relation to DA detection in the presence of both AA and UA, with the aid of a this metal phthalocyanine derivative, together with testing capability in a simulated sample matrix.

2. Materials and methods

2.1 Chemicals

Silver nitrate (99%), sodium citrate (99%), hydrochloric acid (HCl, 37%), sodium hydroxide (98%), uric acid (99%), ascorbic acid (99%), dopamine hydrochloride (98%), sodium chloride (99.5%), sodium nitrate (99%), citric acid (99.5%), calcium chloride (97%) and tetrahydrofuran (99.9%) were all purchased from Sigma Aldrich. Poly(*n*-butyl acrylate) COOH, bis(2-oxo-1,3-oxazolidin-3-yl)phosphinic chloride (99.5%), triethylamine (99.5%), dichlormethane (99.8%), ethanol (99.5%) used were from Merck. All reagent solutions were prepared in double distilled water. Artificial urine samples were prepared according to the recipe provided by Brooks and Keevil.[28] The solution was comprised of 1.1 mM lactic acid (98%), 2.0 mM citric acid (99.5%), 25 mM sodium bicarbonate (99.7%), 170 mM urea (98%), 2.5 mM calcium chloride (97%), 90 mM sodium chloride (99.5%), 2.0 mM magnesium sulphate (99.5%), 10 mM sodium sulphate (99%), 7.0 mM potassium dihydrogen phosphate (99.99%), 7.0 mM dipotassium hydrogen phosphate (99%), and 25 mM ammonium chloride (99.5%) all in Millipore water. The pH of the solution was adjusted to 6.0 *via* the addition of 1.0 M hydrochloric acid (37%).

2.2 Apparatus

Differential pulse, cyclic voltammetry and electrochemical impedance measurements were performed using an electrochemical workstation – CH Instruments Inc. 920, in phosphate buffer (0.1 M, pH 7.2), with a conventional three-electrode cell (5 mL) at room temperature. A modified glassy carbon electrode (3 mm diameter) served as the working electrode, while platinum wire and a standard Ag/AgCl electrode (filled with 3 M KCl) were employed as the counter and reference electrodes, respectively. Prior to electrochemical measurements, the glassy carbon electrode was polished with 1.0, 0.3, and 0.05 μm alumina powders, sonicated in acetone and distilled water and dried at room temperature. All potentials reported are with respect to the Ag/AgCl. Optical absorption spectra were recorded by using a UV-Visible spectrophotometer Model S-2150 UV-Vis spectrophotometer (Spain). Samples were loaded in a quartz cell and measurements were taken over the wavelength range 250–800 nm. In the case of impedance spectroscopy, the amplitude of the applied sine potential of EIS was 25 mV, and a bias potential of 245 mV was fixed as excitation potential. All experiments were performed under the same conditions of room temperature (25 °C) with the modified GCE as working electrode and a VMP3 potentiostat which was monitored by EC-Lab software as impedance analyser.

2.3 Synthesis of Ag NPs using sodium citrate as a reducing agent

Silver nitrate and trisodium citrate were used as starting materials for silver nanoparticle synthesis according to the citrate reduction

method.[29] All reagents were prepared in distilled water. 10 mL of 10 mM sodium citrate was injected rapidly into 100 mL of boiling water containing 1 mM $AgNO_3$ with vigorous stirring. After this, the solution mixture was boiled for approximate 10 minutes, and removed from the hot plate to a cold plate, maintaining stirring until it was cooled to room temperature.[30] In this process, the reaction can be expressed as follows:[31]

$$4Ag^+ + Na_3C_6H_5O_7 + 2H_2O \rightarrow 4Ag + C_6H_8O_7 + 3Na^+ + H^+ + O_2$$

2.4 Synthesis of Cu-Pc-mono amide–PnBA

The ionophore copper monoamine phthalocyanine acrylate (Cu-MAPA) was synthesised by adopting a previously reported procedure[32] with characterisation by elemental analysis, ultraviolet-visible spectroscopy, and infrared spectroscopy. In brief, into a 100 mL two-neck round-bottom flask equipped with a reflux condenser, 2.5 g of poly(*n*-butyl acrylate) COOH, 0.2 g of bis(2-oxo-1,3-oxazolidin-3-yl)phosphinic chloride (BOP-Cl), 0.5 mL of triethylamine, and 50 mL dry CH_2Cl_2 were mixed and stirred under nitrogen at 40 °C. 39.0 mg of purified Cu-Pc mono-amino was dissolved in 20 mL dry CH_2Cl_2 in an addition funnel. The solution was then added drop wise for 30 minutes followed by stirring for 3 h at 70 °C. The reaction mixture was then washed with 30 mL of saturated $NaHCO_3$ solution, 50 mL of saturated NaCl solution (two times), and finally with 100 mL of water. The acrylate polymer, dissolved in 50 mL of dichloromethane and 300 mL of methanol, was then slowly added, precipitating Cu(II) MAPA (see Scheme 1). The product was washed with methanol to ensure the complete removal of non-grafted copper phthalocyanine. The so-produced ionophore was dried under ambient temperature and stored in the dark.

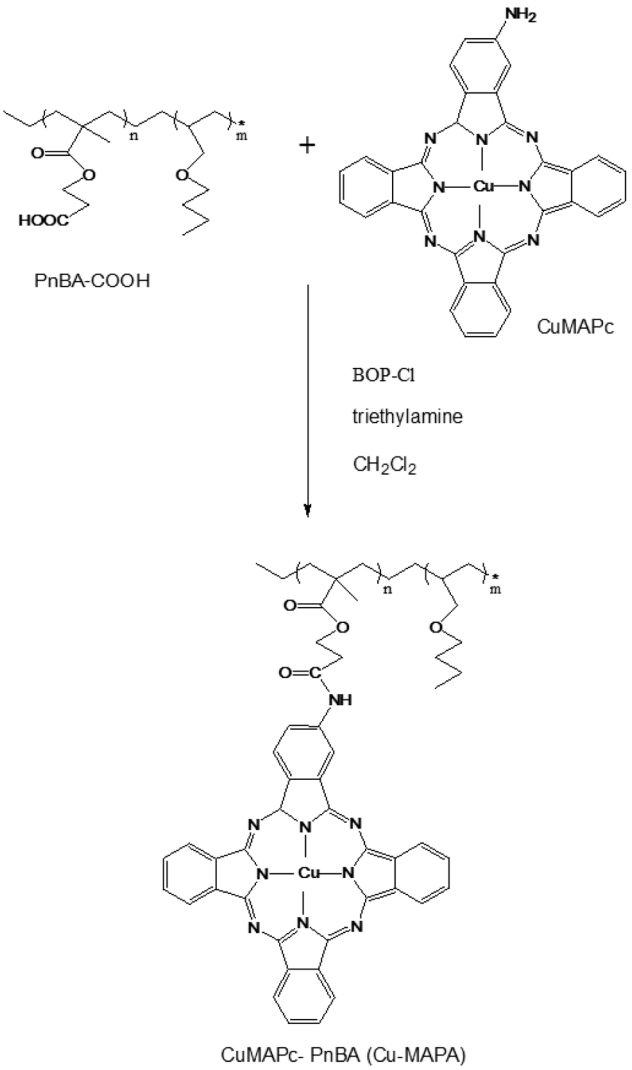

Scheme 1 Synthesis of CuMAPc covalently attached to PnBA–COOH polymer.

2.5 Fabrication of the Cu-MAPA–AgNPs modified glassy carbon electrode

Prior to the sensor fabrication process, glassy carbon (GC) electrodes (diameter 3 mm) were polished with 1.0, 0.3 and 0.05 μm alumina powder, using a polishing cloth with water as the lubricant. The electrodes were then sonicated in distilled water, acetone, ethanol and distilled water in sequence for 5 min each followed by air drying. 1 mg of Cu-MAPA was dissolved in 1 mL THF for 15 min in an ultrasonic bath and the composite film was prepared by dropping 5 μL of the Cu-MAPA suspension onto the GC electrode surface using a micropipette and then evaporating the solvent at room temperature in air. A selected volume of AgNPs was then drop cast onto the surface of the Cu-MAPA/GC electrode (see Scheme 2).

3. Results and discussion

3.1 Optical characterisation

The effect of varying pH on the synthesised AgNPs (pH 6, λ_{max} = 420 nm) was examined and Fig. 1 shows the influence of pH (adjusted using HCl or NaOH) on the absorption peak of AgNPs, with pH 7 resulting in maximum absorption with a slight red shift (between 3–10 nm) at lower pH range due to aggregation.

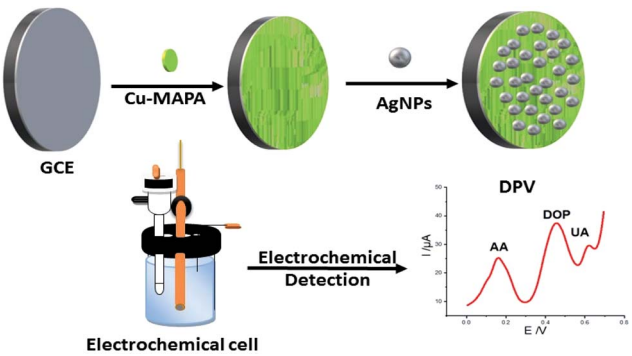

Scheme 2 Electrode modification steps enabling voltammetric separation of the target species.

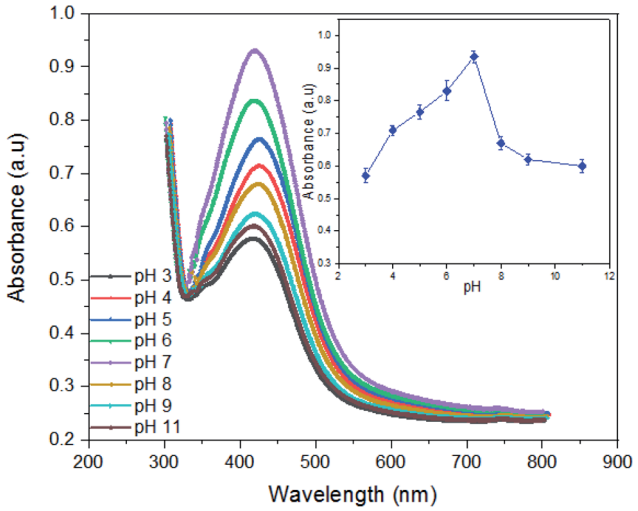

Fig. 1 UV-Visible spectra of synthesised AgNPs, over pH 2–11, (inset) absorbance as the function of solution pH.

With an increase of solution pH (>7), the absorption peak was red-shifted again, probably due to the oxide layer on the surface of AgNPs.[33] The absorption signal was found to reach a maximum at neutral pH.

The UV-Vis absorption spectra of Cu-MAPA in DMF was recorded (Fig. 2 red trace) and results in a shoulder and a peak ($\pi \rightarrow \pi^*$) in the visible region (600–670 nm) corresponding to the Q-band with the splitting and extent of absorption being enhanced in the presence of Ag nanoparticles (Fig. 2 black trace). There was an evident absorption at 320 λ_{max} (Soret B band) which shifted to 350 nm in the presence of Ag NPs.

3.2 Electrochemical characterisation of modified electrodes

Impedance spectroscopy was used to characterise each step of the chemical sensor fabrication and surface modification. The electron transfer resistance (R_{ct}) was found to be proportional to the semicircular diameter at high frequencies[34] (Fig. 3). The Nyquist plots obtained at the bare glassy carbon, in the presence of the Cu-MAPA layer and that of the Cu-MAPA/AgNP modified glassy carbon electrode were modelled according to Randles circuit, using Z_{plot}/Z_{view} software. In this model, generally the R_s represents the resistance of the electrolyte solution in series with the parallel combination of the double layer capacitance C_{dl} and the charge transfer resistance in series with the Warburg impedance Z_ω. In this work, a modified Randles circuit was used to fit the impedance spectra that consist of the active electrolyte resistance R_s in series with the parallel combination of the charge transfer resistance and the double-layer capacitance represented by a constant phase element.

The Nyquist plot of bare GCE (Fig. 3) revealed an R_{ct} of 130 kΩ and a decrease of the impedance transfer charge to 95 kΩ was observed following the deposition of the Cu-MAPA layer. Finally, the deposition of AgNPs, resulted in R_{ct} of 50 kΩ for the electrode which could be attributed to the enhanced conductivity of the AgNPs layer.

The electroactive surface area values of the Cu-MAPA/GCE and AgNPs/Cu-MAPA/GCE were calculated to be 0.36 cm^2 and 0.51 cm^2 respectively using a voltammetric scan rate study in 2 mM $K_3Fe(CN)_6$. The enhancement of the 1 μM dopamine signal shown in Fig. 4 resulted in a 2.2 fold increase in current and a 3.7 fold increase due to the Ag NP, thus confirming the material's contribution to the catalytic oxidation process with resultant signal enhancement (see ESI (1) and (2) for similar data regarding uric acid and ascorbic acid†).

3.3 Electrochemical response of dopamine at modified electrodes

Cyclic voltammetry was used to examine the DOP signal (1 mM in 0.1 M PBS) at bare, Ag NP and Cu-MAPA modified glassy

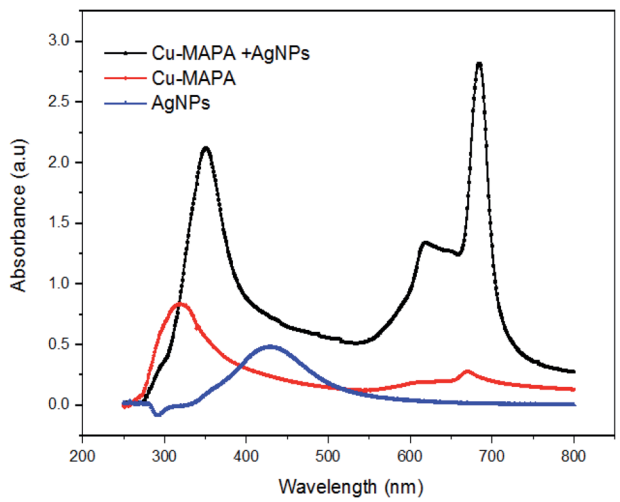

Fig. 2 UV-Vis spectra of AgNPs, Cu-MAPA, and a mixture of AgNPs and Cu-MAPA (4 : 1 v/v).

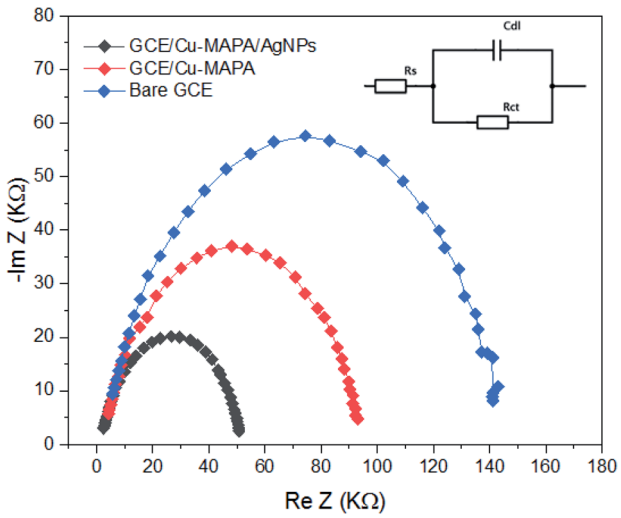

Fig. 3 Nyquist plots of EIS obtained at (blue) bare GCE, (red) Cu-MAPA/GCE and (black) AgNPs/Cu-MAPA/GCE in 1.0 mM $Fe(CN)_6^{3-}$ solution. EIS conditions: frequency range: 100–0.1 kHz; potential: 0.245 V; (inset) modelling circuit.

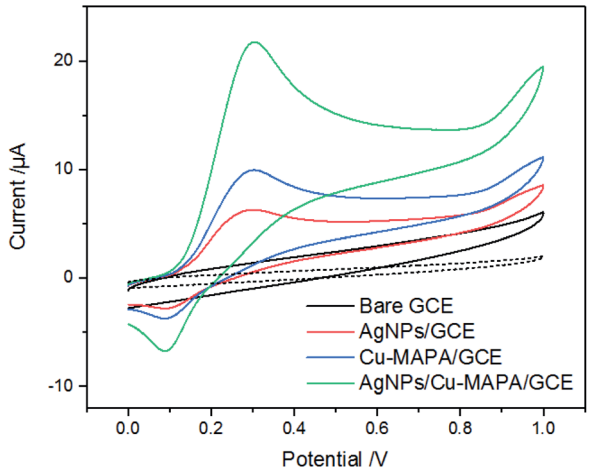

Fig. 4 CVs of 1 µM dopamine prepared in 0.1 M PB (pH 7.4) at bare and modified electrodes GCE, GCE/AgNP, GCE/Cu-MAPA and GCE/Cu-MAPA/AgNP (100 mV s^{-1}). The background CV of the bare electrode was performed in buffer (dashed line).

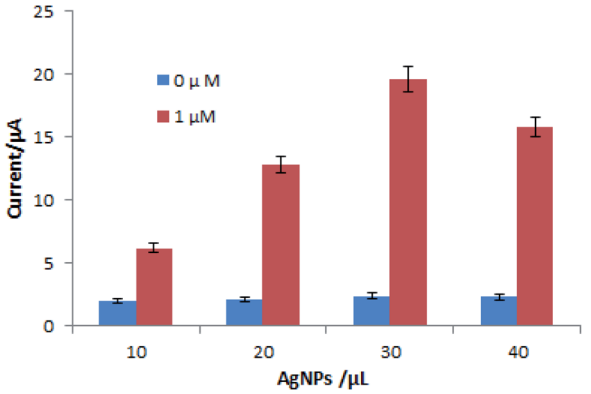

Fig. 5 Optimisation of the loading of AgNPs deposited on the surface of the Cu-MAPA modified GCE in the presence of 1 µM dopamine prepared in 0.1 M phosphate buffer at pH 7.4 with scan rate 100 mV s^{-1} $n = 3$.

carbon electrodes (Fig. 4). A significant enhancement in the magnitude of the anodic electrooxidation response was evident particularly in the case of the Ag-NP/Cu-MAPA modified electrode which exhibited a strong anodic wave at 0.3 V *vs.* Ag/AgCl for the generation of the semiquinone intermediate which resulted in a small cathodic wave upon reduction indicating chemical transformation to the aminochrome product *via* a follow up reaction which involves the nucleophilic amine group. The pK_a of the amino function of dopamine is 10.58 and at the pH employed here (pH 7.2) only a fraction will be in the non-protonated form and it is possible that the Cu-MAPA/AgNP composite may have some influence on the stability of the initial oxidation product (pH study shown in ESI (3) and ESI (4) shows data for scan rate study in 1 µM dopamine†).

The effect of the quantity of AgNPs (10 to 40 µL) immobilised on the surface of the Cu-MAPA modified glassy carbon electrode was examined in order to establish any influence on the electrocatalytic dopamine response. Increasing the concentration of AgNPs enhances both anodic ($E_p = 310$ mV) and cathodic ($E_p =$ 8 mV) peak. However, levels >40 µL led to possible saturation which correspondingly decreased the electron transfer rate. Therefore, an optimised level of 30 µL was selected for further analysis (see Fig. 5).

The proposed electrocatalytic interaction between the nanocomposite modified surface and the dopamine molecule is shown below where Cu-MAPA is capable of accelerating the oxidation of dopamine to the quinone product (a $2H^+$, $2e^-$ process).

$$\text{Cu(II)-MAPA} \rightarrow \text{Cu(III)-MAPA} + e^-$$

$$2\text{Cu(III)-MAPA} + \text{dopamine} \rightarrow 2\text{Cu(II)-MAPA} + \text{dopamine quinone} + 2H^+$$

In order to perform quantitative dopamine analysis, differential pulse voltammetric (DPV) was employed and a graph of the anodic peak current ($I_{p(a)}$) at $E_p = 280$ mV *vs.* dopamine concentration is shown in Fig. 6. A 10 fold enhancement in peak current was obtained relative to control (unmodified) and Cu-MAPA/GCE responses. The electrocatalytic oxidation of DA was carried out at the AgNPs/Cu-MAPA/GCE by varying its concentration from 5 to 30 µM. A linear relationship (inset Fig. 6) resulted over the range 10 nM to 10 µM with regression equation $I_{p(a)}$ (µA) = 9.22 + (±0.54) + 20.75 (±0.67). The correlation coefficient was $R^2 =$ 0.9736 and detection limit (LOD) and quantification limit (LOQ) were calculated as 0.7 nM and 2.3 nM respectively using IUPAC (International Union of Pure and Applied Chemistry) definitions.

$$\text{LOD}_{SA} = \frac{3S_b}{q} \quad (1)$$

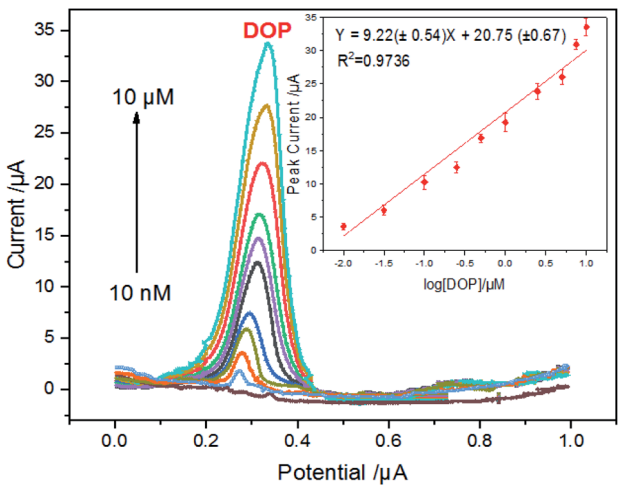

Fig. 6 DPV voltammograms of DOP at AgNPs/Cu-MAPA/GCE, from 10 nM to 10 µM (including background signal at modified electrode). Inset: plot of oxidation current *versus* DOP concentration prepared in 0.1 M PBS (pH 7.2). The scan rate and amplitude of the DPV pulse were 50 mV s^{-1} and 25 mV, respectively.

Table 1 Comparative study of the performance of reported modified electrodes for the determination of DOP[a]

Electrode	pH	Detection limit (nM)	Linear range (μM)	Ref.
Pd/PEDOT/rGO	7.0	140	1–200	35
AuNPs/MoS_2/GCE	7.2	80	3–115	36
Pd/CNF/carbon paste electrode	7.0	200	0.5–160	37
Au/PE/PS/BDDa	7.2	250	5–100	38
PANI/Au nano-electrode	6.8	100	0.3–200	39
PEDOT/GO	7.0	39	0.1–175	40
g-CN/GCE	7.4	10	5–600	41
AgNPs/CuMAPA/GCE	**7.2**	**0.7**	**0.01–10**	**This work**

[a] Poly(3,4-ethylenedioxythiophene) functionalised reduced graphene oxide with palladium nanoparticles (Pd/PEDOT/rGO), molybdenum disulfide (MoS_2) and gold nanoparticles (AuNPs) AuNPs@MOS_2/GCE, gold nanoparticles and polyelectrolyte (PE) on polystyrene (PS)-modified boron-doped diamond (BDD) electrode, poly(3,4-ethylenedioxythiophene) (PEDOT) doped with graphene oxide (GO), polyaniline/Au nanocomposite (PANI/Au nanoelectrode), graphitic carbon nitride polymers (g-CN).

$$\mathrm{LOQ_{SA}} = \frac{10S_b}{q} \quad (2)$$

where S_b is the standard deviation of the blank signal and q is the slope of the calibration curve.

A comparison of the analytical performance (sensitivity, LOD, linear response range and selectivity) of the developed sensor with previously reported dopamine sensors has been made – see Table 1.

It can be concluded that the developed sensor showed superior performance in more than one category compared with previously reported similar electrodes systems for dopamine determination.

3.4 Electrochemical response of uric acid at modified electrodes

DPV analysis was conducted over a range of 10 nM to 10 μM uric acid as shown in Fig. 7. The oxidation peak current (E_p = 558 mV) was observed to increase with increasing concentration of uric acid – see inset for current *vs.* log uric acid relationship.

Direct proportionality between the analyte concentration and current signal was evident from the data (inset Fig. 7.) over a wide concentration range studied. The linear relationships are given by the following equation: Y = 7.61 + (±0.52) + 15.42 (±0.55). The correlation coefficient R^2 = 0.9593 and the detection limit (LOD) and quantification limit (LOQ) were calculated at 2.5 nM and 9 nM respectively.

3.5 Electrochemical response of ascorbic acid at modified electrodes

Fig. 8 shows that the DPV response of ascorbic acid at the modified glassy carbon electrode over the range 10 nM to 100 μM in 0.1 M phosphate buffer pH 7.5. A graph of the anodic peak current ($I_{p(a)}$) taken at E_p = 152 mV *vs.* ascorbate concentration is plotted as inset.

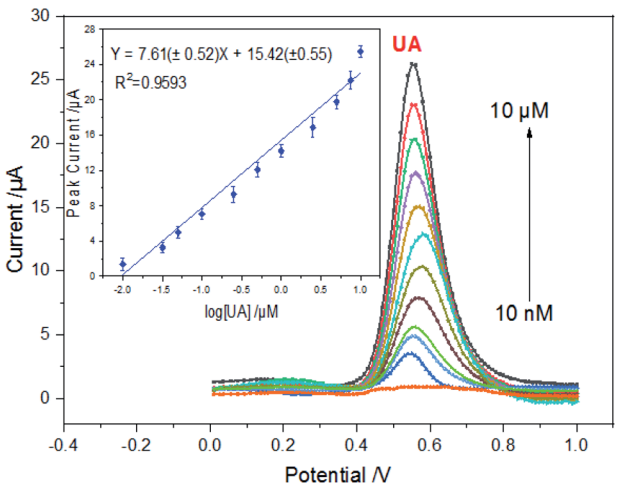

Fig. 7 DPV voltammograms of UA at AgNPs/Cu-MAPA modified GCE, from 10 nM to 10 μM (including background signal in electrolyte). Inset: plot of oxidation current *versus* UA concentrations prepared in 0.1 M phosphate buffer (pH 7.2). The scan rate and amplitude of the DPV pulse were 50 mV s^{-1} and 25 mV, respectively.

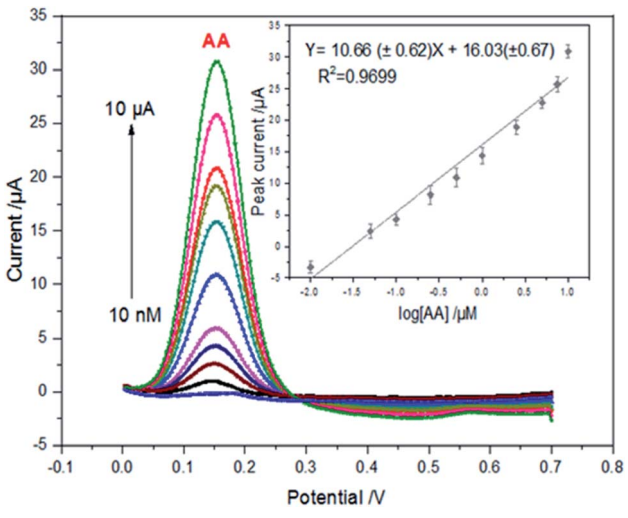

Fig. 8 DPV voltammograms of AA from 10 nM to 10 μM (including background signal in electrolyte) at AgNPs/Cu-MAPA modified GCE. Inset: plot of oxidation current *versus* AA concentration prepared in 0.1 M phosphate buffer (pH 7.2). The scan rate and amplitude of the DPV pulse were 50 mV s^{-1} and 25 mV, respectively.

Table 2 Summary analytical performance of the dopamine, uric acid and ascorbic acid sensors based on electrocatalytic oxidation signals at AgNP/Cu-MAPA modified GCEs

	Dopamine	Uric acid	Ascorbic acid
Linear range (μM)	0.01–10	0.01–10	0.01–10
Limit of detection (nM) (3σ/slope)	0.7	2.5	5.0
RSD (%) $n = 3$	3.22	4.12	3.70
R^2	0.9703	0.9593	0.9699

The oxidation peak current (E_p = 152 mV) for different concentrations of ascorbic acid was measured from the equivalent oxidation peak after baseline correction. The oxidation peak current of AA linearly increased over the response range from 10 nM to 10 μM (inset Fig. 8). The linear relationship is given by the following equation: $Y = 10.66 + (\pm 0.62) + 16.03$ (± 0.67). The correlation coefficient was $R^2 = 0.9699$. The limit of detection (LOD) was calculated to be 5 nM.

In order to estimate the fabrication reproducibility of the AgNPs/Cu-MAPA modified electrode, the relative standard deviations (% RSD) of five electrodes prepared independently and used to measure 0.5 μM DOP and 0.5 μM UA, 0.5 μM of AA was calculated to be 3.22%, 4.12% and 3.70% respectively, providing evidence of good intra electrode precision. Analytical performance data for the responses to the three individual target analytes is summarised in Table 2 below.

3.6 Simultaneous determination of DOP, UA and AA

Following the individual electrochemical detection of the neurotransmitters, simultaneous detection of ascorbic acid and uric acid was performed using differential pulse voltammetry with data shown in Fig. 9. Two well-defined anodic peaks at ~+0.158 V and 0.63 V *vs.* Ag/AgCl were observed with good separation achieved. The modified GCE electrodes were capable of providing good resolution for the two neurotransmitters as may be observed from the selective oxidation peaks of uric acid and ascorbic acid.

The electro-oxidation processes of DOP and UA in a mixture where the concentration of one species changed, while the other species was kept constant were also investigated with data shown in Fig. 10. The concentration of dopamine was varied over the range 0.5–50 μM while uric acid was kept constant at 0.5 μM.

Fig. 10 data demonstrates that the peak current of DAP was proportional to concentration, which was increased from 0.5 μM to 50 μM while keeping the concentration of UA fixed at 0.5 μM. There were minimal changes in the peak current and peak potential for UA. These results show that the peaks remain well separated and that DOP and UA can be simultaneously detected in a mixed system at the GCE/Cu-MAPA/AgNPs surface.

Simultaneous determination of all three species using DPV was carried out over the potential range −0.2 to 1.0 V *vs.* Ag/AgCl (as shown in Fig. 11). Three well-defined peaks at 155, 420, and 630 mV *vs.* Ag/AgCl were observed, corresponding to the differential pulse voltammograms of AA, DOP and UA, respectively. Peaks separations of 265 mV and 210 mV between DOP–AA and DOP–UA respectively allowed quantitation of the species over the range 0.5–100 μM. The anodic shift of DOP (approx. 150 mV) which occurred in the presence of AA and UA may result from chemical interactions in solution. These could include (a) H bonding interactions between DOP and AA (or UA) making it less amenable to oxidation; this could also be a reason for the

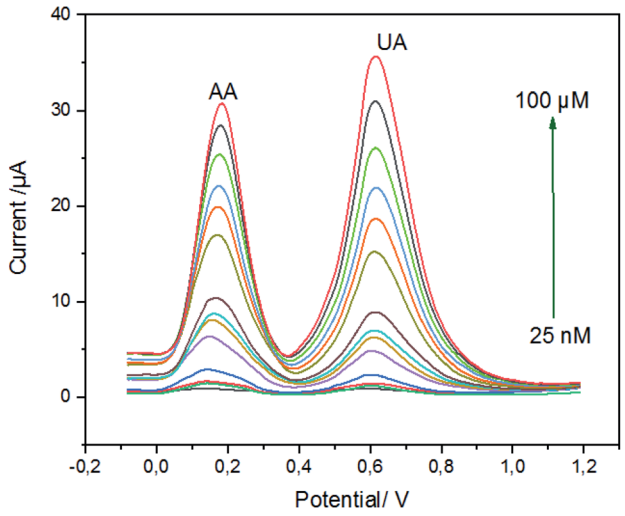

Fig. 9 Differential pulse voltammograms of AA and UA at AgNPs/Cu-MAPA/GCE in a 0.1 M phosphate buffer (pH 7.2) over the range 25 nM to 100 μM. Other conditions as before.

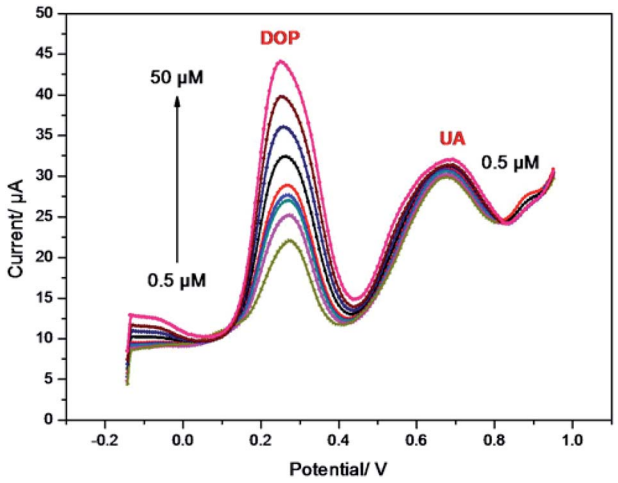

Fig. 10 DPV voltammograms of DA at AgNPs/Cu-MAPA modified GCE in the presence of 0.5 μM UA in phosphate buffer, pH 7.2.

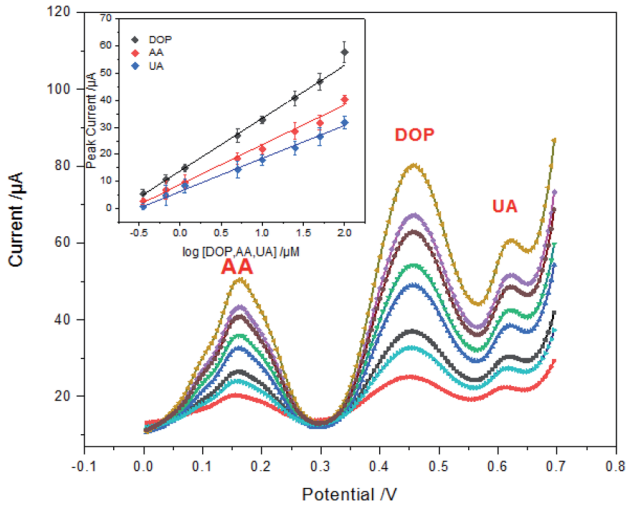

Fig. 11 DPV voltammograms at AgNPs/CuMAPA/GCE in 0.1 M phosphate buffer (pH 7.4) containing increasing concentrations (0.5–100 μM) of AA, DOP and UA. Inset: plot of oxidation current *versus* DOP, AA and AA concentration. The scan rate and amplitude of the DPV pulse were 50 mV s^{-1} and 25 mV, respectively.

Table 3 Influence of selected interferences on peak currents (μA) for DOP (0.5 μM) UA (1 μM) and AA (1 μM) at AgNPs/Cu-MAPA/GCE (response shown is average of $n = 3$ measurements)

Interfering ions	Dopamine	Uric acid	Ascorbic acid
No interferent	6.83 (±0.37)	14.37 (±0.79)	6.61 (±0.82)
Sodium chloride	6.12 (±0.12)	13.49 (±0.18)	6.31 (±0.21)
Sodium nitrate	6.23 (±0.41)	13.75 (±0.38)	6.47 (±0.66)
Citric acid	6.06 (±0.62)	13.67 (±0.19)	6.21 (±0.39)
Calcium chloride	5.94 (±0.78)	13.52 (±0.62)	6.11 (±0.41)

Table 4 Actual and measured concentration of AA, DOP and UA in the artificial urine sample ($n = 3$)

Actual concentration AA, DOP, UA (μM)	AA measured concentration (μM)	DOP measured concentration (μM)	UA measured concentration (μM)
0.5	(0.492 ± 0.09)	(0.521 ± 0.002)	(0.472 ± 0.011)
1	(0.96 ± 0.06)	(1.21 ± 0.31)	(1.6 ± 0.07)
10	(10.2 ± 0.23)	(9.25 ± 0.52)	(10.72 ± 0.03)

evident peak broadening; (b) the reducing properties of AA could influence the oxidised fraction of DOP in the cell; no significant change in sensitivity was evident in the presence of AA and UA.

Simultaneous determination studies were also performed using silver nanoparticle-decorated reduced graphene oxide modified electrode for ascorbic acid, dopamine, uric acid and tryptophan[42] and Afraz *et al.*[43] describe the modification of a carbon paste electrode (CPE) with multiwalled carbon nanotubes (MWCNTs) and an ionic liquid (IL) as an approach for simultaneous determination of AA, DA and UA. In other work, a sensor based on graphene quantum dots/ionic liquid modified screen-printed carbon electrode for AA, DOP, and UA simultaneous determination was developed by Kunpatee *et al.* 2020.[44] Compared with the reports in literature to date, the methodology and data presented here is promising for reliable and sensitive applications in bioanalysis, exhibiting good peak to peak separation. Moreover, covalent binding of the copper phthalocyanine mono amino molecule to the acrylate polymer is expected to provide improved film stability with a 6% decrease in electroactivity (following 20 cycles), contributing to enhanced analytical performance.

Sensor performance over time was determined by measuring the current response of the Cu-MAPA/AgNPs modified glassy carbon electrode. After 7 days, 8.6% of the current signal was lost with daily measurement of a 1 μM mixture of the three analytes (AA, DOP and UA). This illustrates the robust nature of the Cu-MAPA/AgNPs modified glassy carbon electrode for the purpose of detecting neurotransmitters.

3.7 Interference study

The influence of various interferences which may coexist in real samples was carried out. It was found that a 200-fold excess of sodium chloride, sodium nitrate, citric acid, calcium chloride did not interfere with the determination of AA, DA and UA. The functionalised electrode was tested for individual and simultaneous determination of AA, DA and UA in the presence of large quantities of interferent species using DPV. It was found that 200-fold excess of these ions did not result in any false positive or negative effect on the target analyte oxidation signal. The tolerance limit was defined as the maximum concentration of the interfering substance that causes an error <5% for the determination of DOP, UA and AA (see Table 3 for data generated).

3.8 Sample analysis

In order to evaluate the applicability of the proposed method for the determination of DOP, UA and AA in real samples, an artificial urine solution was prepared for testing using the method of standard addition. Recovery values obtained are shown Table 4 varying from 94% to 107%, providing evidence that the proposed method to simultaneously determine DOP, AA and UA in simulated samples was possible with good analytical data generated.

4. Conclusions

The method proposed here confirmed that enhanced surface to area volume ratio provided by Ag nanoparticles in the presence of the electrocatalytic species Cu-MAPA enabled simultaneous electrochemical and determination of dopamine, ascorbic acid and uric acid by means of DPV. The AgNPs/Cu-MAPA modified GCE was shown to have good electrochemical catalytic activity for the electrooxidation of the species with an enhancement of analytical signal and reduction in the overpotential relative to studies at bare electrodes. Sensitivity values were 14.43 ± 2.44,

14.86 ± 3.85 and 9.82 ± 1.74 μA μM^{-1} for DOP, AA and UA respectively. Performance data over clinically relevant ranges, surface reproducibility and capability for measurement in a simulated urine matrix provide for a promising sensing strategy for these co-existing species.

Conflicts of interest

There are no conflicts to declare.

Acknowledgements

This work was partially supported by the European Commission 7th Framework Programme Marie Curie Actions IRSES FP7-PEOPLE-2012-IRSES N° 318053 318053: SMARTCANCERSENS project and the NATO Science for Peace (SFP) Project CBP.NUKR.SFP 984173.

References

1 R. D. Blakely, *Science*, 2001, **293**, 2407–2409.
2 H. R. Zare and N. Nasirizadeh, *Sens. Actuators, B*, 2010, **143**, 666–672.
3 J. A. Drisko, J. Chapman and V. J. Hunter, *J. Am. Coll. Nutr.*, 2003, **22**, 118–123.
4 C. R. Raj, F. Kitamura and T. Ohsaka, *Analyst*, 2002, **127**, 1155–1158.
5 M. Noroozifar, M. Khorasani-Motlagh and A. Taheri, *Talanta*, 2010, **80**, 1657–1664.
6 X. Liu, Y. Peng, X. Qu, S. Ai, R. Han and X. Zhu, *J. Electroanal. Chem.*, 2011, **654**, 72–78.
7 Y. Bu and S.-W. Lee, *J. Nanosci. Nanotechnol.*, 2013, **13**, 5992–5996.
8 A. Wu, W. Cheng, Z. Li, J. Jiang and E. Wang, *Talanta*, 2006, **68**, 693–699.
9 L. Zhang and X. Jiang, *J. Electroanal. Chem.*, 2005, **583**, 292–299.
10 H. Vidya, B. E. Kumara Swamy and M. Schell, *J. Mol. Liq.*, 2016, **214**, 298–305.
11 M. A. Khalilzadeh and M. Borzoo, *J. Food Drug Anal.*, 2016, **24**, 796–803.
12 B. Kaur, T. Pandiyan, B. Satpati and R. Srivastava, *Colloids Surf., B*, 2013, **111**, 97–106.
13 Y. V. M. Reddy, S. Bathinapatla, T. Łuczak, M. Osińska, H. Maseed, P. Ragavendra, L. S. Sarma, V. V. S. S. Srikanth and G. Madhavi, *New J. Chem.*, 2018, **42**, 3137–3146.
14 Y. V. M. Reddy, B. Sravani, H. Maseed, T. Łuczak, M. Osińska, L. SubramanyamSarma, V. V. S. S. Srikanth and G. Madhavi, *New J. Chem.*, 2018, **42**, 16891–16901.
15 A. Zawadzka, P. Płóciennik, J. Strzelecki, A. Korcala, A. K. Arof and B. Sahraoui, *Dyes Pigm.*, 2014, **101**, 212–220.
16 M. Szybowicz, W. Bała, K. Fabisiak, K. Paprocki and M. Drozdowski, *J. Mater. Sci.*, 2011, **46**, 6589–6595.
17 A. Zawadzka, P. Płóciennik, I. Czarnecka, J. Sztupecka and Z. Łukasiak, *Opt. Mater.*, 2012, **34**, 1686–1691.
18 X. Zuo, H. Zhang and N. Li, *Sens. Actuators, B*, 2012, **161**, 1074–1079.
19 F. Cruz Moraes, M. F. Cabral, S. A. S. Machado and L. H. Mascaro, *Electroanalysis*, 2008, **20**, 851–857.
20 Z. Fredj, M. Ben Ali, M. N. Abbas and E. Dempsey, *Anal. Chim. Acta*, 2019, **1057**, 98–105.
21 S. Pakapongpan, J. P. Mensing, D. Phokharatkul, T. Lomas and A. Tuantranont, *Electrochim. Acta*, 2014, **133**, 294–301.
22 R. Seoudi and H. A. Althagafi, *Silicon*, 2018, **10**, 2165–2171.
23 M. C. DeRosa and R. J. Crutchley, *Coord. Chem. Rev.*, 2002, **233–234**, 351–371.
24 M. E. Wieder, D. C. Hone, M. J. Cook, M. M. Handsley, J. Gavrilovic and D. A. Russell, *Photochem. Photobiol. Sci.*, 2006, **5**, 727–734.
25 V. P. Chauke, W. Chidawanyika and T. Nyokong, *Electroanalysis*, 2011, **23**, 487–496.
26 T. Nyokong and E. Antunes, *Coord. Chem. Rev.*, 2013, **257**, 2401–2418.
27 P. Alessio, C. S. Martin, J. A. de Saja and M. L. Rodriguez-Mendez, *Sens. Actuators, B*, 2016, **233**, 654–666.
28 T. Brooks and C. W. Keevil, *Lett. Appl. Microbiol.*, 1997, **24**, 203–206.
29 P. C. Lee and D. Meisel, *J. Phys. Chem.*, 1982, **86**, 3391–3395.
30 Y. Bu and S.-W. Lee, *J. Nanosci. Nanotechnol.*, 2013, **13**, 5992–5996.
31 M. G. Guzmán, J. Dille and S. Godet, *Int. J. Metall. Mater. Sci. Eng.*, 2008, **2**, 91–98.
32 M. N. Abbas, A. L. A. Radwan, N. M. Nooredeen and M. A. A. El-Ghaffar, *J. Solid State Electrochem.*, 2016, **20**, 1599–1612.
33 R. A. Alvarez-Puebla and R. F. Aroca, *Anal. Chem.*, 2009, **81**, 2280–2285.
34 J. Martinovic, J. van Wyk, S. Mapolie, N. Jahed, P. Baker and E. Iwuoha, *Electrochim. Acta*, 2010, **55**, 4296–4302.
35 J. E. Choe, M. S. Ahmed and S. Jeon, *J. Electrochem. Soc.*, 2016, **163**, B113.
36 S. Su, H. Sun, F. Xu, L. Yuwen and L. Wang, *Electroanalysis*, 2013, **25**, 2523–2529.
37 J. Huang, Y. Liu, H. Hou and T. You, *Biosens. Bioelectron.*, 2008, **24**, 632–637.
38 M. Wei, L.-G. Sun, Z.-Y. Xie, J.-F. Zhii, A. Fujishima, Y. Einaga, D.-G. Fu, X.-M. Wang and Z.-Z. Gu, *Adv. Funct. Mater.*, 2008, **18**, 1414–1421.
39 Y. Zhang, L. Lin, Z. Feng, J. Zhou and Z. Lin, *Electrochim. Acta*, 2009, **55**, 265–270.
40 W. Wang, G. Xu, X. T. Cui, G. Sheng and X. Luo, *Biosens. Bioelectron.*, 2014, **58**, 153–156.
41 T. Jiang, G. Jiang, Q. Huang and H. Zhou, *Mater. Res. Bull.*, 2016, **74**, 271–277.
42 B. Kaur, T. Pandiyan, B. Satpati and R. Srivastava, *Colloids Surf., B*, 2013, **111**, 97–106.
43 A. Afraz, A. A. Rafati and M. Najafi, *Mater. Sci. Eng., C*, 2014, **44**, 58–68.
44 K. Kunpatee, S. Traipop, O. Chailapakul and S. Chuanuwatanakul, *Sens. Actuators, B*, 2020, **314**, 128059.